Received: 19 July 2022 | Revised: 12 January 2022 | Accepted: 5 December 2022 | Published on: 28 February 2023

DOI: 10.1002/gamm.202300002

ORIGINAL PAPER

Interpolation-based parametric model order reduction of automotive brake systems for frequency-domain analyses

Fabian Matter[1] | **Igor Iroz**[2] | **Peter Eberhard**[1]

[1]Institute of Engineering and Computational Mechanics, University of Stuttgart, Stuttgart, Germany

[2]Dr. Ing. h.c. F. Porsche Aktiengesellschaft, Stuttgart, Germany

Correspondence
Peter Eberhard, Institute of Engineering and Computational Mechanics, University of Stuttgart, Pfaffenwaldring 9, 70569 Stuttgart, Germany
Email: peter.eberhard@itm.uni-stuttgart.de

Abstract

Brake squeal describes noise with different frequencies that can be emitted during the braking process. Typically, the frequencies are in the range of 1 to 16 kHz. Although the noise has virtually no effect on braking performance, strong attempts are made to identify and eliminate the noise as it can be very unpleasant and annoying. In the field of numerical simulation, the brake is typically modeled using the Finite Element method, and this results in a high-dimensional equation of motion. For the analysis of brake squeal, gyroscopic and circulatory effects, as well as damping and friction, must be considered correctly. For the subsequent analysis, the high-dimensional damped nonlinear equation system is linearized. This results in terms that are non-symmetric and dependent on the rotational frequency of the brake rotor. Many parameter points to be evaluated implies many evaluations to determine the relevant parameters of the unstable system. In order to increase the efficiency of the process, the system is typically reduced with a truncated modal transformation. However, with this method the damping and the velocity-dependent terms, which have a significant influence on the system, are neglected for the calculation of the eigenmodes, and this can lead to inaccurate reduced models. In this paper, we present results of other methods of model order reduction applied on an industrial high-dimensional brake model. Using moment matching methods combined with parametric model order reduction, both the damping and the various parameter-dependent terms of the brake model can be taken into account in the reduction step. Thus, better results in the frequency domain can be obtained. On the one hand, as usual in brake analysis, the complex eigenvalues are evaluated, but on the other hand also the transfer behavior in terms of the frequency response. In each case, the classical and the new reduction method are compared with each other.

KEYWORDS

brake squeal, model order reduction, damped systems, vibration analysis, complex eigenvalue analysis

1 | INTRODUCTION

Brake squeal is a noise emitted by vibrations of the brake system. The system is excited by frictional forces that occur between the rotor and the brake pads during braking, and yields thus a self-excited vibration that reaches a limit cycle. An entire braking system, an example is shown in Figure 1, can be excited to oscillate. Thereby, the noise emission can come from different components. The causes of the noise are investigated using various methods. Mostly, laboratory experiments and complex numerical simulations or simple minimal models, which try to reproduce a certain effect of brake squeal, are used for this purpose. An overview of different methods and especially numerical methods can be found in [13], [17], and [11] respectively. For the numerical methods, the brake system is modeled with linear finite elements. This leads to the equation of motion

$$\boldsymbol{M}\ddot{\boldsymbol{q}} + \hat{\boldsymbol{D}}\dot{\boldsymbol{q}} + \hat{\boldsymbol{K}}\boldsymbol{q} = \boldsymbol{f}, \tag{1}$$

where $\boldsymbol{M}$, $\hat{\boldsymbol{D}}$, and $\hat{\boldsymbol{K}} \in \mathbb{R}^{n\times n}$ are the mass matrix, the damping matrix and the stiffness matrix, respectively. The coefficient matrices are time invariant, parameter-dependent and real, large and sparsely populated with nonzero entries. The vector $\boldsymbol{f}$ is the vector of external forces, and $\boldsymbol{q}$ is the vector of the displacements and $\dot{\boldsymbol{q}}, \ddot{\boldsymbol{q}}$ are its time derivatives. In this work, only the dependency of the system on the rotational speed of the rotor $\Omega \in [\Omega_{\min}, \Omega_{\max}]$ is considered. For the identification of self-excited vibrations we have $\boldsymbol{f} = \boldsymbol{0}$ and the vibrational modes can be investigated based on the eigenvalues λ and the eigenvectors $\boldsymbol{\Phi}$ following from the quadratic eigenvalue problem (QEVP)

$$(\lambda^2\boldsymbol{M} + \lambda\hat{\boldsymbol{D}} + \hat{\boldsymbol{K}})\boldsymbol{\Phi} = \boldsymbol{0}. \tag{2}$$

This analysis is very common in the industry and is called complex eigenvalue analysis (CEA). According to classical linear stability analysis [8], the equilibrium is stable, if the real parts of all eigenvalues are negative. However, the equilibrium is unstable when at least one real part is positive or there are multiple purely imaginary eigenvalues with zero real part. The object of the CEA is to determine the eigenvalues, which have a positive real part and are therefore in the right half-plane. Additionally, the large QEVP has to be solved for many parameter values Ω, which is very challenging, even nowadays. For this reason, Model Order Reduction (MOR) is used to reduce the computational effort. Therefore, our large scale system from Equation (1) is transformed in to a smaller system by projection. In the state of art procedure, a modal truncation is used for calculating a projection matrix. However, in this step some damping terms are neglected for the calculation of the projection basis. With the presented method, all terms are considered. Furthermore, with the interpolation-based approach it is possible to have a reduced system with a good quality of

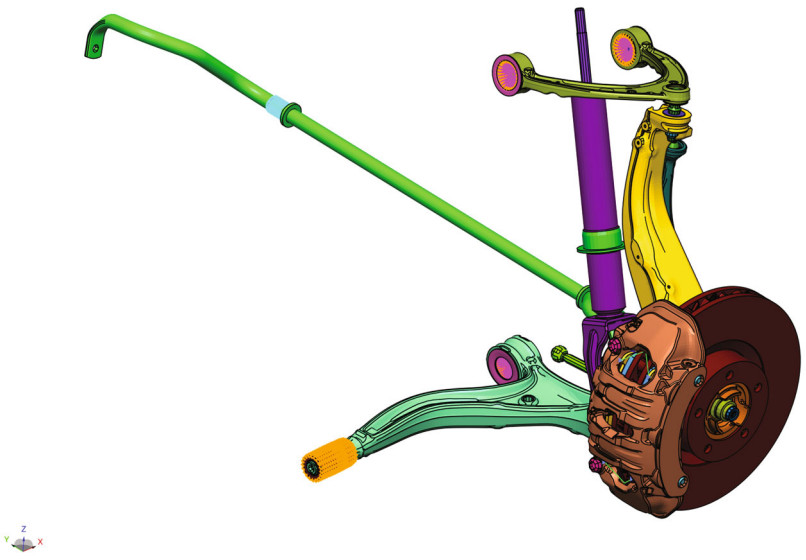

FIGURE 1 Example of a detailed brake model including the parts mounted in the suspension corner of the vehicle.

approximation over the whole parameter space, which is not possible with the classical modal truncation of the undamped system.

The paper has the following structure. In Section 2, we present and discuss the state of the art procedure of modeling and analyzing a brake model with regard to instabilities. In the subsequent Section 3, the Model Order Reduction techniques are described. At first, the traditional modal truncation and afterwards a new parametric approach with Kylov-subspaces is presented. In Section 4 the simulation results of an industrial brake model are presented. Not only the eigenvalues but also the transfer functions of the models are compared. On the basis of the transfer functions, which are calculated for the entire parameter space, the reduction methods can also be evaluated.

2 | MODELING PROCEDURE

It is the aim of the modeling, to obtain a system that can be used to make predictions about the stability and vibration behavior of the braking system. For this purpose, the modeling of the braking system is carried out at the macro level, as it is usual for flexible mechanical components. As a consequence the Finite Element method is applied. This provides a mathematical model that describes the structural dynamics of the physical system. However, nonlinearities such as the contact forces or the rotor rotation are not taken into account at the first moment. Therefore, several steps must be performed that allow to take into account the nonlinearities such as the contact forces or the rotation of the disc. Afterwards we achieve a linearized system, which enables the application of the linear stability analysis. This procedure is also implemented in commercial software packages, such as Permas. The following explanations of the modeling steps are based on [10].

In the first step, the linear equation of motion is obtained from this modeling. Neglecting external forces it leads to

$$\boldsymbol{M}\ddot{\boldsymbol{q}} + \boldsymbol{D}\dot{\boldsymbol{q}} + \boldsymbol{K}\boldsymbol{q} = \boldsymbol{0}, \tag{3}$$

where $\boldsymbol{M}$ is the mass matrix, $\boldsymbol{D}$ is the damping matrix and $\boldsymbol{K}$ is the elastic stiffness matrix. Information on calculation of these matrices can be found in any classical FE-textbook for example, in [22].

2.1 | Static contact analysis

In the next step, we extend our model from Equation (3) with normal and friction forces in the contact area. Therefore, an iterative nonlinear static contact analysis is performed. A pressure is applied on the pistons, which are pressing the brake pads on the brake rotor. This allows the detection of the contact areas and the calculation of the normal forces. To consider friction forces in our model, a velocity field is applied on the brake rotor and tangential forces are calculated with a friction law, for example, Coulomb [18]. As a consequence, the brake system deforms. In Figure 2 the unloaded state, the deformed state, and the tangential forces are shown. To consider this state in our model, Equation (3) is extended with two terms. We achieve

$$\boldsymbol{M}\ddot{\boldsymbol{q}}_{\xi} + \left(\boldsymbol{D} + \frac{1}{\Omega}\boldsymbol{D}_{\Omega}\right)\dot{\boldsymbol{q}}_{\xi} + (\boldsymbol{K} + \boldsymbol{Q})\boldsymbol{q}_{\xi} = \boldsymbol{0}. \tag{4}$$

Thereby describes $\frac{1}{\Omega}\boldsymbol{D}_{\Omega}$ the matrix of friction-induced damping and $\boldsymbol{Q}$ the circulatory effects, where $\boldsymbol{D}_{\Omega}$ is symmetric and $\boldsymbol{Q}$ is nonsymmetric. A detailed description of the path and velocity dependent terms can be found in [9] and [7]. In addition, the detected contacts are frozen and closed with multi-point constraints (MPCs). At this stage the coordinates $\boldsymbol{q}$ no longer describe the unloaded system, but $\boldsymbol{q}_{\xi}$ the displacement of the linearized, loaded state, shown in Figure 2. The following steps are based on this state.

2.2 | Quasi-static analysis with centrifugal loads

In the modeling step before, the rotation of the brake disc is modeled as a rigid body movement to calculate the velocities in the contact zones, which in turn are used for the calculation of the friction forces. The next step is again about the

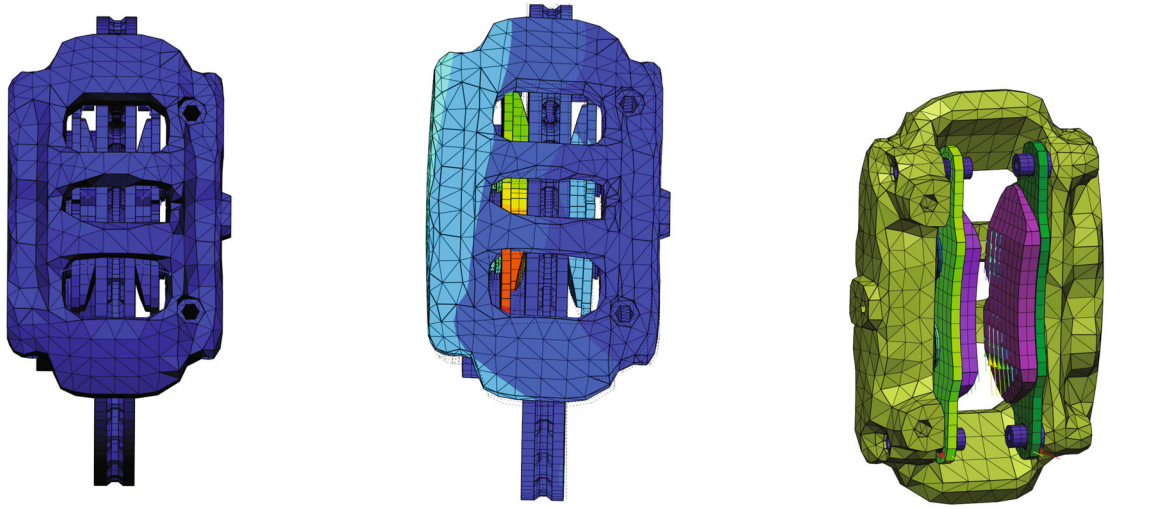

(A) Unloaded brake system (B) Deformed brake system due to contact forces (C) Distribution of friction forces on the brake pad

FIGURE 2 Different views of the brake system in the modeling procedure.

rotation of the rotor. The model described in Equation (4) is extended with geometric stiffness and gyroscopic terms. Due to the rotation, the stiffness and damping of the initial system are changing. But instead of moving the nodes, a load of centrifugal forces is applied on the system. With this method the internal stress condition can be determined and the additional terms $\frac{\Omega^2}{\Omega_{\text{ref}}^2}\boldsymbol{K}_\Omega \boldsymbol{q}_\xi$ and $\frac{\Omega}{\Omega_{\text{ref}}}\boldsymbol{G}\dot{\boldsymbol{q}}_\xi$ can be determined. It results

$$\boldsymbol{M}\ddot{\boldsymbol{q}}_\xi + \underbrace{\left(\boldsymbol{D} + \frac{\Omega_{\text{ref}}}{\Omega}\boldsymbol{D}_\Omega + \frac{\Omega}{\Omega_{\text{ref}}}\boldsymbol{G}\right)}_{\hat{\boldsymbol{D}}}\dot{\boldsymbol{q}}_\xi + \underbrace{\left(\boldsymbol{K} + \frac{\Omega^2}{\Omega_{\text{ref}}^2}\boldsymbol{K}_\Omega + \boldsymbol{Q}\right)}_{\hat{\boldsymbol{K}}}\boldsymbol{q}_\xi = \boldsymbol{0}. \tag{5}$$

The matrix $\boldsymbol{K}_\Omega$ is symmetric and is describing the geometric stiffness, whereas $\boldsymbol{G}$ is skew-symmetric and includes the gyroscopic effects. Details for the calculation can be found in [10,19]. The resulting deformation of the system can be seen in Figure 3. The steps described are necessary to linearize the nonlinear brake model at an operating sliding point and thus enable the use of stability theory and frequency-domain analysis. The resulting system is now the basis for the subsequent investigations.

2.3 | Calculation of the eigenvalues

As usual in the field of brake acoustics analysis, it is assumed that the brake squeal is caused by an instability of the equilibrium solution $\boldsymbol{q}_\xi \equiv 0$ of Equation (5). This means that we need to calculate the eigenvalues with a positive real part, because then the damping ratio is negative. For the calculation we use Equation (5) and with the ansatz function

$$\boldsymbol{q}_\xi = \boldsymbol{\Phi}_j e^{\lambda_j t} \tag{6}$$

it results the quadratic eigenvalue problem

$$(\lambda_j^2 \boldsymbol{M} + \lambda_j \hat{\boldsymbol{D}} + \hat{\boldsymbol{K}})\boldsymbol{\Phi}_j = \boldsymbol{0}. \tag{7}$$

Thereby $\boldsymbol{\Phi}_j$ are the complex eigenvector and $\lambda_j = \rho_j \pm \mathrm{i}\omega_j$ the conjugate pair of complex eigenvalues. Before a complex eigenvalue analysis is performed, a projection to a smaller subspace is processed. This is needed to reduce the computational effort. More details on model reduction are explained later in Section 3. At this point, however, it should be

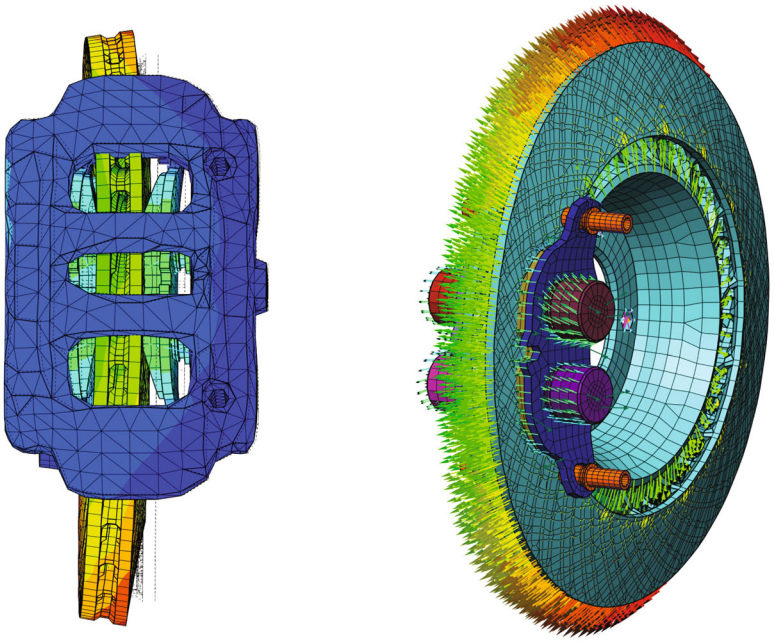

(A) Deformed brake model under centrifugal loads (B) Vectorial representation of the load

FIGURE 3 Deformed brake-model under centrifugal loads according to the second modeling step.

mentioned that the choice of the projection is crucially important for the quality of the approximation and that the calculation of the basis is also complex. However, compared to the massive memory and computational requirements of a full eigenvalue analysis, the effort is justified. So we have more effort in the calculation of the basis, but save efforts in the eigenvalue calculation, which has to be repeated for many parameter points. The projection of the system matrices given by

$$\left\{\tilde{\boldsymbol{M}}, \tilde{\boldsymbol{D}}, \tilde{\boldsymbol{K}}\right\} = \boldsymbol{V}^{\intercal} \left\{\boldsymbol{M}, \hat{\boldsymbol{D}}, \hat{\boldsymbol{K}}\right\} \boldsymbol{V}. \tag{8}$$

For the analysis, a linearization approach transforms the quadratic eigenvalue problem of size n into an equivalent linear eigenvalue problem of double dimension $2n$ with the same eigenvalues λ_j. Due to the properties of the system matrices, in many implementations a linearization with the form

$$\left(\lambda_j \begin{bmatrix} \tilde{\boldsymbol{M}} & \boldsymbol{0} \\ \boldsymbol{0} & \tilde{\boldsymbol{I}} \end{bmatrix} + \begin{bmatrix} \tilde{\boldsymbol{D}} & \tilde{\boldsymbol{K}} \\ \tilde{\boldsymbol{I}} & \boldsymbol{0} \end{bmatrix}\right) \begin{bmatrix} \lambda_j \tilde{\boldsymbol{\Phi}}_j \\ \tilde{\boldsymbol{\Phi}}_j \end{bmatrix} = \boldsymbol{0} \tag{9}$$

is chosen. With the help of the projection and the linearization, the eigenvalues λ_j and eigenvectors $\tilde{\boldsymbol{\Phi}}_j$ of the quadratic eigenvalue problem are calculated. The eigenvectors can be back projected from the reduced, modal space to the physical, nodal space with

$$\boldsymbol{\Phi_j} = V \tilde{\boldsymbol{\Phi}}_j. \tag{10}$$

As already figured out in the calculation steps, our linearized system is dependent on the parameter Ω. Therefore, the quadratic eigenvalue problem has to be solved for each parameter.

2.4 | Calculation of the transfer function

Tools and analysis methods from systems theory can be usefully employed in the simulative investigation and analysis of the deformation behavior of elastic structures. In Equation (1) the vector of the external forces can often be written as

$$\boldsymbol{f}(t) = \boldsymbol{B}\boldsymbol{u}(t). \tag{11}$$

Thereby, $\boldsymbol{B} \in \mathbb{R}^{N\times r}$ denotes the input matrix and $\boldsymbol{u} \in \mathbb{R}^r$ the vector of the system inputs. With the help of the input matrix, the system inputs are distributed to the elastic structure. Following the same scheme, the deformation $\boldsymbol{q}$ of the system is mapped on the system output $\boldsymbol{y}(t) \in \mathbb{R}^h$ through

$$\boldsymbol{y}(t) = \boldsymbol{C}\boldsymbol{q}(t). \tag{12}$$

Thereby, $\boldsymbol{C} \in \mathbb{R}^{h\times N}$ is the output matrix. Applying Equation (11) and (12) to the equation of motion (1) we achieve the system

$$\begin{aligned} \boldsymbol{M}\ddot{\boldsymbol{q}}(t) + \widehat{\boldsymbol{D}}(t)\dot{\boldsymbol{q}} + \widehat{\boldsymbol{K}}\boldsymbol{q}(t) &= \boldsymbol{B}\boldsymbol{u}(t), \\ \boldsymbol{y}(t) &= \boldsymbol{C}\boldsymbol{q}(t). \end{aligned} \tag{13}$$

Alternatively, the system can be described in the complex variable domain by

$$\begin{aligned} s^2\boldsymbol{M}\boldsymbol{Q}(s) + s\widehat{\boldsymbol{D}}\boldsymbol{Q}(s) + \widehat{\boldsymbol{K}}\boldsymbol{Q}(s) &= \boldsymbol{B}\boldsymbol{U}(s), \\ \boldsymbol{Y}(s) &= \boldsymbol{C}\boldsymbol{Q}(s). \end{aligned} \tag{14}$$

Here, s is the Laplace-variable and $\boldsymbol{Q}(\boldsymbol{s})$, $\boldsymbol{U}(\boldsymbol{s})$ and $\boldsymbol{Y}(\boldsymbol{s})$ are the Laplace-transforms of the vector of displacements, the vector of system inputs and the vector of system outputs, respectively. By transforming Equation (14) to $\boldsymbol{Q}(\boldsymbol{s})$ and inserting the lower part of the Equation (14), the following representation is obtained

$$\boldsymbol{Y}(s) = \boldsymbol{C}(s^2\boldsymbol{M} + s\widehat{\boldsymbol{D}} + \widehat{K})^{-1}\boldsymbol{B}\boldsymbol{U}(s). \tag{15}$$

The matrix-valued function

$$\boldsymbol{H}(s) = \boldsymbol{C}(s^2\boldsymbol{M} + s\widehat{\boldsymbol{D}} + \widehat{K})^{-1}\boldsymbol{B} \quad \in \mathbb{C}^{h\times r} \tag{16}$$

is the so called transfer function, which maps the system inputs on to the system outputs. For an evaluation along the imaginary axis with $s = \mathrm{i}w$, this corresponds to the frequency response matrix, [12]. Each entry of the transfer matrix then gives both phase and magnitude information about how much harmonic sinusoidal excitation signals are amplified when propagated through the system. As with the calculation of the eigenvalues, reduced matrices $\tilde{\boldsymbol{M}}, \tilde{\boldsymbol{D}}, \tilde{\boldsymbol{K}}$ can also be used for the calculation of the transfer function.

In this contribution the analyzed system is a multiple input multiple output (MIMO)-system. In this case, matrix norms can be used to represent the frequency-dependent transmission in a single number. A common option is the so-called Frobenius norm, see [1,21]. It is calculated as

$$||\boldsymbol{H}(f,\Omega)||_{\mathrm{F}} = \sqrt{\sum_{j=1}^{h}\sum_{k=1}^{r}|H_{j,k}(f,\Omega)|^2}. \tag{17}$$

The matrix norm allows a representation of the transmission behavior of a MIMO-system as a scalar quantity depending on the frequency, which in turn allows the quantification of the response characteristic.

3 | MODEL ORDER REDUCTION

For detailed brake models, as in Figure 1, the resulting parametric equation system (5) has many degrees of freedom. In combination with many parameter values, the computational effort for calculating the eigenvalues or the transfer functions of the models, becomes very computationally intensive. Therefore, the model order reduction by projection provides a great benefit at this point. Here, the model is projected onto a smaller subspace and the following applies

$$\boldsymbol{q} \approx \boldsymbol{V}\tilde{\boldsymbol{q}} \quad \text{with} \quad \boldsymbol{q} \in \mathbb{R}^N \quad \text{and} \quad \tilde{\boldsymbol{q}} \in \mathbb{R}^n, \; n \ll N. \tag{18}$$

Here $\boldsymbol{q}$ are the elastic coordinates of the displacement, $\tilde{\boldsymbol{q}}$ the reduced elastic coordinates, and $\boldsymbol{V}$ the projection matrix. An important point of the MOR is to set up a projection matrix $\boldsymbol{V}$, so that the number of reduced DOFs is significantly smaller than the DOFs of the full system, while still approximating well the desired behavior of the system. However, a reduction error always arises, which must be kept as small as possible. In the last decade, several methods have been developed and investigated for this purpose, as they can be found for example in [4,14].

In the field of brake analysis, the modal truncation method is typically used for the reduction. Here, the behavior of the system is approximated by eigenmodes from the undamped system. Thus, an attempt is made to approximate the behavior of a damped system with the modes of an undamped system. This results in a significant error due to the reduction, which can be reduced with newer interpolation-based approaches. Interpolation-based methods for parametric systems are explained for example in [2].

3.1 | Traditional modal reduction

Modal reduction attempts to represent the dynamic behavior of a system with the natural modes. For this purpose, either free eigenmodes or modes of the clamped system are used. In the CEA method the columns of the projection matrix $\boldsymbol{V}_{\text{mod}}$ are eigenvectors of the full, undamped system. In the context of this brake analysis a simplified eigenvalue problem at reference speed Ω_{ref},

$$(\lambda_j^2 \boldsymbol{M} + \hat{\boldsymbol{K}}_{\text{ref}})\boldsymbol{\Phi}_j = \boldsymbol{0}, \tag{19}$$

is used to calculate the eigenvectors. Some related modes are illustrated in Figure 4. Consequently, no damping terms or terms dependent on the parameter Ω are taken into account. Hence, the following applies for the modal projection matrix

$$\boldsymbol{V}_{\text{mod}} = [\boldsymbol{\Phi}_1, \boldsymbol{\Phi}_2, \boldsymbol{\Phi}_3, \; \dots \; , \boldsymbol{\Phi}_n] \in \mathbb{R}^{N \times n} \tag{20}$$

corresponding to the first n eigenvalues. Then, for the reduced linearized equation of motion

$$\tilde{\boldsymbol{M}}\ddot{\boldsymbol{q}}_\xi + \tilde{\boldsymbol{D}}\dot{\boldsymbol{q}}_\xi + \tilde{\boldsymbol{K}}\boldsymbol{q}_\xi = \boldsymbol{0} \tag{21}$$

applies with the matrices

$$\tilde{\boldsymbol{M}} = \boldsymbol{V}_{\text{mod}}^{\mathsf{T}} \boldsymbol{M} \boldsymbol{V}_{\text{mod}}, \quad \tilde{\boldsymbol{D}} = \boldsymbol{V}_{\text{mod}}^{\mathsf{T}} \hat{\boldsymbol{D}} \boldsymbol{V}_{\text{mod}}, \quad \text{and} \quad \tilde{\boldsymbol{K}} = \boldsymbol{V}_{\text{mod}}^{\mathsf{T}} \hat{\boldsymbol{K}} \boldsymbol{V}_{\text{mod}}. \tag{22}$$

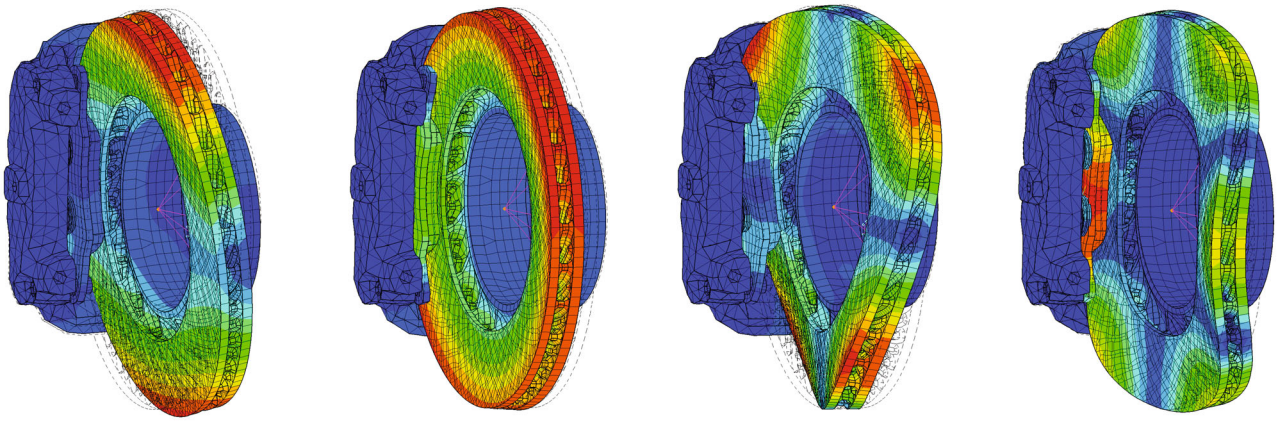

(A) Mode shape at 551 Hz (B) Mode shape at 736 Hz (C) Mode shape at 976 Hz (D) Mode shape at 1892 Hz

FIGURE 4 Mode shapes of the undamped brake system used for the modal reduction basis.

3.2 | New parametric approach

As already described in Section 2, the system matrices in Equation (5) depend on the rotational velocity Ω of the disc, making the equation of motion into a parameter dependent system. In the last years, also methods for model order reduction of such parameter dependent system have been developed, see [3]. Contrary to linear model order reduction, parametric model order reduction methods take the parameter dependency into account already during the reduction step. This leads to parameter dependent, reduced models which still exhibit the parameter dependency and often show a good approximation behavior over a user-defined frequency range and over a user-defined parameter range.

This contribution uses so-called interpolatory projection methods for parameterized system, see [2] for first order and, for example, [20] for second order systems. The parameter dependent equation of motion (5) is first rewritten as a linear, second order, parameterized input-output system

$$\begin{aligned} \boldsymbol{M}\ddot{\boldsymbol{q}}_\xi + \hat{\boldsymbol{D}}(\Omega)\dot{\boldsymbol{q}}_\xi + \hat{\boldsymbol{K}}(\Omega)\boldsymbol{q}_\xi &= \boldsymbol{B}\boldsymbol{u}, \\ \boldsymbol{y} &= \boldsymbol{C}\boldsymbol{q}_\xi. \end{aligned} \tag{23}$$

Then a system input $\boldsymbol{u}$ is added describing external forces on the system, which are distributed onto the structure using the input matrix $\boldsymbol{B}$. The system output matrix $\boldsymbol{C}$ extracts the displacements of interest $\boldsymbol{y}$ from the structure. The input-output behavior of system (23) can also be described in frequency domain with the transfer function

$$\boldsymbol{H}(\omega, \Omega) = \boldsymbol{C}\left(-\omega^2\boldsymbol{M} + \mathrm{i}\omega\hat{\boldsymbol{D}}(\Omega) + \hat{\boldsymbol{K}}(\Omega)\right)^{-1}\boldsymbol{B}. \tag{24}$$

Computing a projection matrix for the discrete frequency expansion point σ_j and the discrete parameter expansion point Ω_j

$$\boldsymbol{V}_{\mathrm{int}} = \mathrm{span}\left[\left(-\sigma_j^2\boldsymbol{M} + \mathrm{i}\sigma_j\boldsymbol{D}(\Omega_j) + \boldsymbol{K}(\Omega_j)\right)^{-1}\boldsymbol{B}\right] \tag{25}$$

and reducing the system matrices as

$$\tilde{\boldsymbol{M}} = \boldsymbol{V}_{\mathrm{int}}^{\mathsf{T}}\boldsymbol{M}\boldsymbol{V}_{\mathrm{int}}, \quad \tilde{\boldsymbol{D}}(\Omega) = \boldsymbol{V}_{\mathrm{int}}^{\mathsf{T}}\hat{\boldsymbol{D}}(\Omega)\boldsymbol{V}_{\mathrm{int}}, \quad \tilde{\boldsymbol{K}}(\Omega) = \boldsymbol{V}_{\mathrm{int}}^{\mathsf{T}}\hat{\boldsymbol{K}}(\Omega)\boldsymbol{V}_{\mathrm{int}}, \tag{26}$$

$$\tilde{\boldsymbol{B}} = \boldsymbol{V}_{\mathrm{int}}^{\mathsf{T}}\boldsymbol{B} \quad \text{and} \quad \tilde{\boldsymbol{C}} = \boldsymbol{C}\boldsymbol{V}_{\mathrm{int}} \tag{27}$$

ensures that the reduced transfer function

$$\tilde{\boldsymbol{H}}(\omega, \Omega) = \tilde{\boldsymbol{C}}\left(-\omega^2\tilde{\boldsymbol{M}} + \mathrm{i}\omega\tilde{\boldsymbol{D}}(\Omega) + \tilde{\boldsymbol{K}}(\Omega)\right)^{-1}\tilde{\boldsymbol{B}} \tag{28}$$

is matched to the full order transfer function as

$$\tilde{\boldsymbol{H}}(\sigma_j, \Omega_j) = \boldsymbol{H}(\sigma_j, \Omega_j) \tag{29}$$

at the selected expansion points σ_j and Ω_j. Reduction with interpolatory methods, therefore, allows the user to reduce parameterized systems such that the transfer function of the full and of the reduced order system coincide exactly at a user-defined expansion point. Furthermore, it is possible to evaluate Equation (25) multiple times for multiple parameter values and frequency expansion points and to concatenate the results. Doing so ensures that the reduced and the full order transfer function match at all expansion points. Selecting a sufficiently large number of expansion points yields reduced systems which approximate the original system dynamics well on the entire frequency and parameter range. For more information on interpolatory projection methods, the reader is referred to [2,20]

3.2.1 | Implementation details of parametric approach

In this section some details of the implementation of the new parametric model order reduction (pMOR) approach are explained. The algorithm used to calculate the projection basis and reduce the system is shown in Algorithm 1. Besides

Algorithm 1. Calculate subspace for pMOR and reduce system

Input: system matrices $\boldsymbol{M}, \boldsymbol{D}, \boldsymbol{D_\Omega}, \boldsymbol{G}, \boldsymbol{K}, \boldsymbol{K_\Omega}, \boldsymbol{Q}, \boldsymbol{C}, \boldsymbol{B}$, vector of rotational velocities $\boldsymbol{\Omega}$, vector of expansion points $\boldsymbol{s}$, vectors J_b, J_c, frequency vector $\boldsymbol{f}$, reference frequency f_{ref}

Output: $\boldsymbol{M_{red}}, \boldsymbol{D_{red}}, \boldsymbol{K_{red}}, \boldsymbol{B_{red}}, \boldsymbol{C_{red}}$

1: **for** $i = 1 : n_\Omega$ **do**
2: compute $\boldsymbol{M}, \widehat{\boldsymbol{D}}, \widehat{\boldsymbol{K}}$ for Ω_i as in Equation (5)
3: compute $\boldsymbol{V_i}$ with expansion points $\boldsymbol{s}$ using Dual Rational Arnoldi-Method
4: **end for**
5: $\boldsymbol{V} = [\boldsymbol{V_1}, \boldsymbol{V_2}, \dots, \boldsymbol{V_i}]$
6: compute SVD and sort $[\boldsymbol{U}, \boldsymbol{Singval}, W] = \text{svd}(\boldsymbol{V}, 'econ')$;
7: $\boldsymbol{Singval} = \boldsymbol{Singval}/\boldsymbol{Singval}(1)$;
8: $\boldsymbol{SingvalKept} = \boldsymbol{Singval} > tol$;
9: $\boldsymbol{V} = \boldsymbol{U}(:, \boldsymbol{SingvalKept})$;
10: project into Subspace as in Equation (26)

the system matrices, some more parameters are necessary, i.e., the vector of the rotational velocities Ω, parameters for the Dual Rational Arnoldi-method s, J_b, J_c and the reference frequency f_{ref}. The calculation of the basis is done in a loop over all chosen velocities.

In the first step, the system is constructed for Ω_i and afterwards the Krylov vectors for the chosen expansion points s are computed. The choice of these parameters is decisive for the size of the reduced system and the quality of the approximation. In line 5 the global basis is constructed by concatenation. In line 6 an economic-size singular value decomposition is done, because the left-singular vectors for the new basis are used. The left-singular vectors with the related singular value, which are smaller than the defined tolerance *tol* are removed from the system, see line 9. In the last step, in line 10, the system matrices are reduced according to Equation (26).

4 | SIMULATION RESULTS

In the following, investigations for an automotive disc brake model are shown. The model has a more realistic geometry as the model used in [16]. It consists of multiple parts such as the brake rotor, caliper, brake pads, and pistons. The caliper is designed as a fixed caliper and has four pistons for pressing the two pads onto the rotor. The rotor has a thickness of 30 mm and an outer diameter of 330 mm. The model is meshed with different elements and it results in a model with 103 822 degrees of freedom (DOF). More information are listed in Table 1. The caliper has a fixation at the nodes marked in blue, see Figure 5 and for the calculation of the reduction basis and the transfer function a system input and output is defined. The red marked node on the disc is defined as the input and the red marked node on the caliper is defined as the output of the system. Since the brake squeal occurs at low driving speeds, the rotational disc parameter Ω is selected from 0.5 to 20 rad/s. With a tire-dimension of 305/30R20 this corresponds to a velocity of the car of 0.2 to 8 km/h.

To compare the computation time, all simulations are made on the same desktop-PC with an AMD Ryzen 9 5950X 16-Core processor and 128GB RAM.

TABLE 1 Properties of several components of the disc brake.

Component	Material	Type	Degrees of freedom
Rotor	Cast iron	Isotropic	46 k
Pads	Composite	Orthotropic	3.1 k
Caliper	Aluminum	Isotropic	45 k
Piston	Aluminum	Isotropic	1.0 k

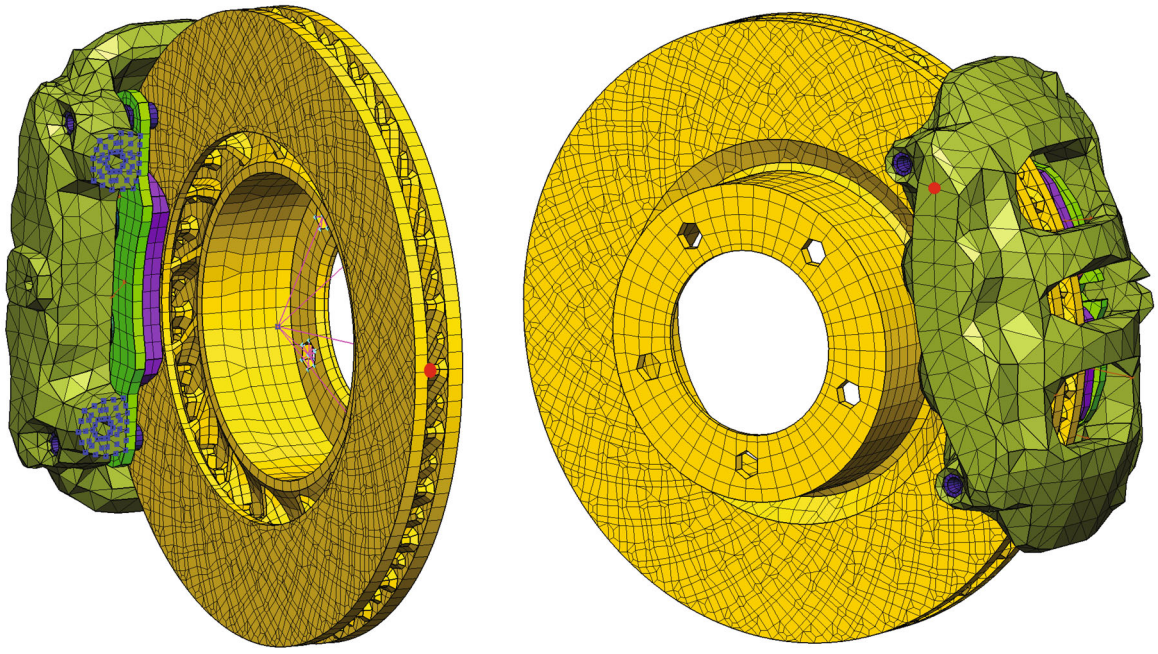

(A) Detailed view with fixed nodes in blue an the output in red

(B) Detailed view with fixed nodes in blue an the input in red

FIGURE 5 Industrial brake system with four-piston caliper.

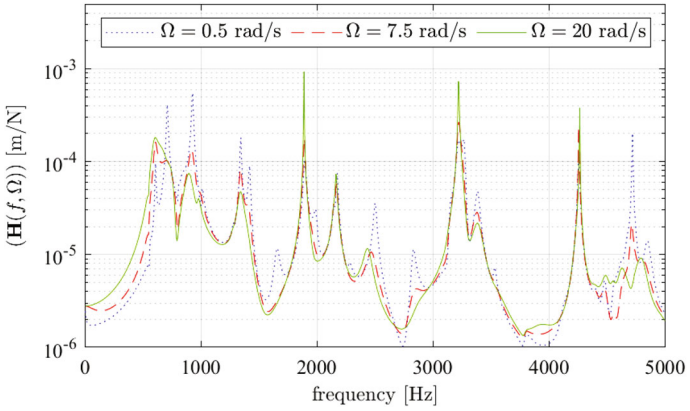

FIGURE 6 Frobenius norm of the transfer function $||\boldsymbol{H}(f,\Omega)||_{\mathrm{F}}$ of the full system.

4.1 | Comparison of the transfer function

In order to evaluate the dynamic behavior, the transfer behavior is often analyzed. Therefore, the transfer function of the brake model is calculated in the following section. In addition to the evaluation of the dynamic behavior, the quality of the reduced model can also be assessed on the basis of the transmission error. The nodes described in Figure 5 are used as input and output. The excitation of the system is in the out-of-plane direction of the disc. At the output node, all three DOFs are considered. The calculation of the transfer function for the full system is very computationally expensive and is shown for three rotational speeds in Figure 6. It can be seen that the frequency of the dominant eigenfrequencies remains the same, but the amplitude varies significantly with the rotation speed. For example, in the range of 700 Hz, a strong peak can be seen at $\Omega = 0.5$ rad/s. With increasing speed, however, this peak becomes smaller. But one cannot say that with increasing velocities the natural frequencies are more damped. For example, at 1900 or 3200 Hz, the amplitude increases with increasing speed. Thus, the parameter dependence on the speed is also very well recovered in the transfer function.

In Figure 7 and Figure 8 the transfer functions for the whole parameter range of $\Omega_j = \{0.5 : 0.5 : 20\}$ are shown. The rotation speed is plotted on the Y-axis and the amplification on the Z-axis. Here one can see again clearly how the system changes depending on the rotational speed Ω. In order to be able to compare the transfer function of the reduced system with the full system, an error of the transfer function is calculated according to

$$\varepsilon(f, \Omega) = \frac{||\boldsymbol{H}(f, \Omega) - \tilde{\boldsymbol{H}}(f, \Omega)||_{\mathrm{F}}}{||\boldsymbol{H}(f, \Omega)||_{\mathrm{F}}}. \tag{30}$$

This allows a better assessment of the quality of the model or the reduction method. For the modal reduced model 300 eigenmodes to the 300 lowest eigenvalues were used, which corresponds to a frequency range over 20 kHz. This results in a reduced system dimension of $n = 300$. In Figure 9 the error of the transfer function of the modally reduced model is shown. It can be seen that the error is large in the entire parameter range, and is also frequently larger than 10%. At low frequencies up to about $f = 2000$ Hz, the error is slightly smaller than at higher frequencies. This is possibly due to the fact that the first 300 eigenmodes are used for the reduction and thus the low frequency behavior can

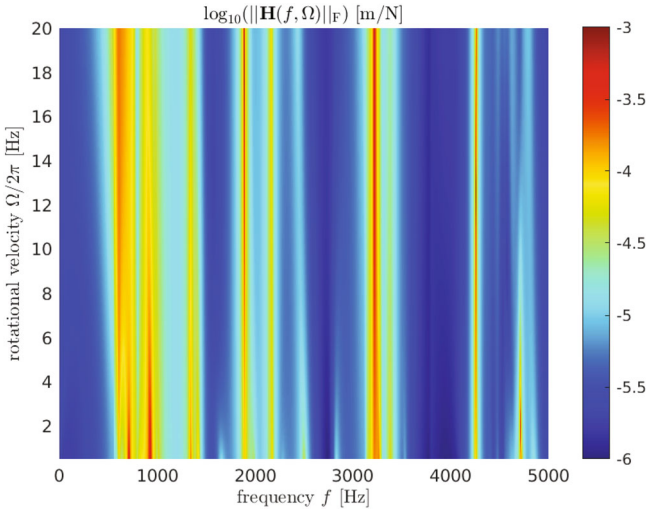

FIGURE 7 Logarithm of the Frobenius norm of the transfer function $||\boldsymbol{H}(f, \Omega)||_{\mathrm{F}}$ of the full system.

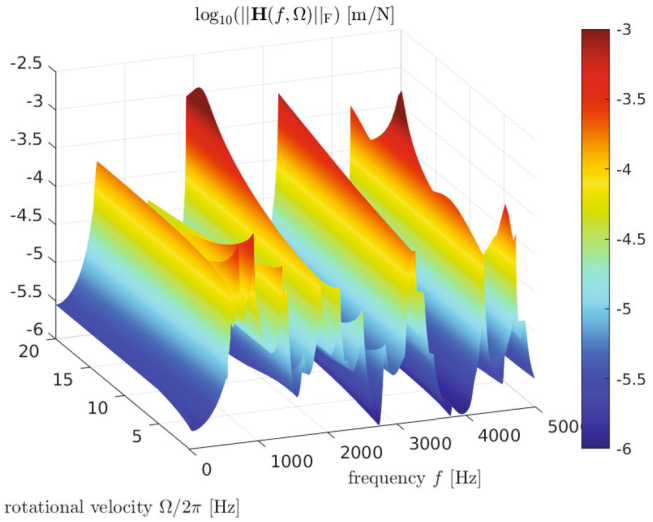

FIGURE 8 Iso-view of the transfer function $||\boldsymbol{H}(f, \Omega)||_{\mathrm{F}}$ of the full system.

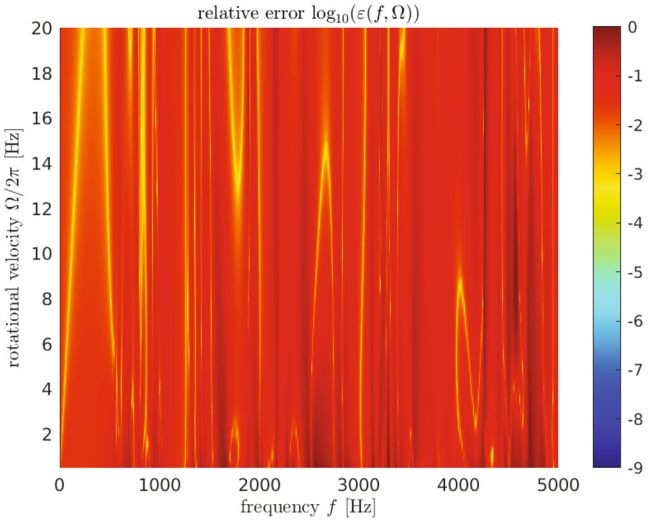

FIGURE 9 Relative error $\varepsilon(f,\Omega)$ of the transfer function of the modally reduced system.

be better approximated. The time for computing the modal basis was 97 s, the time to calculate the transfer function was 51 s.

In the reduction with the interpolation-based approach, the following parameters were chosen $\Omega_j = \{1 : 3 : 20\}$ and $s = \{250 : 250 : 10\,000\}2\pi\mathrm{j}$. This results in a basis of size $n = 560$ in the first step. However, by the singular value decomposition and excluding basis vectors that have low independence, the effective size is reduced to $n = 326$, which is comparable in size to the modal basis. The resulting error of the transfer function of the pMOR-reduced system is shown in Figure 10. By using the same scale for the error, it is immediately noticeable that it is significantly smaller over the entire parameter range. Only in a few places the error becomes larger than 1%. Since the calculation of the basis is based on the approximation of the transfer function at certain expansion points s, the error is especially small at these points. These can be recognized as small blue places in Figure 10. The computation time for the pMOR basis is roughly 21 min and the computation of the transfer function is similar to the modal reduced transfer function with 60 s. The modal reduction is with 97 s in the advantage compared with the parametric reduction with 21 min for the computation of the basis. When calculating the transfer function, the difference of the reduced system is rather small. But even considering the time to calculate the reduction bases, the calculation times for both methods are very small compared to the calculation time of the full system with about 3 days.

4.2 | Complex eigenvalues

The brake squeal is attributed to eigenvalues with a positive real part of the linearized system. Therefore, we can perform a full dense analysis of the reduced system with MATLAB's function polyeig to calculate the eigenvalues. We use the same system as described in Section 4, also the reduced systems are the same. But for the full system the computation is very memory and computing intensive and the used PC with 128 GB memory is not sufficient. There are other solution methods to solve QEVPs more efficiently as described in [5,6]. However, in this work we calculate the residual of the selected computed eigenvalues and vectors with

$$r((\lambda_j, \boldsymbol{\Phi}_j) = \frac{||(\lambda_j^2\boldsymbol{M} + \lambda_j\boldsymbol{D} + \boldsymbol{K})\boldsymbol{\Phi})_j||_\infty}{||\ (|\lambda_j|^2|\boldsymbol{M}| + |\lambda_j||\boldsymbol{D}|| + |\boldsymbol{K}|)|\boldsymbol{\Phi}_j|\ ||_\infty} \tag{31}$$

to evaluate the accuracy of the investigated reduction methods.

In the following, we are interested in the eigenvalues in the rectangular domain $\mathcal{R}$, which is defined by $-3 < \mathrm{Re}(\lambda) < 100$ and $0 < \mathrm{Im}(\lambda) < 31416$. The imaginary part corresponds to 5000 Hz, as used for the transfer functions in Section 4.1. In Figure 11 we can see the results of the eigenvalue analysis for different rotational speeds $\Omega = \{7.5, 10, 20, 40\}$ rad/s. In addition to the representation of the eigenvalues in the complex plane, these are color-coded depending on the calculated

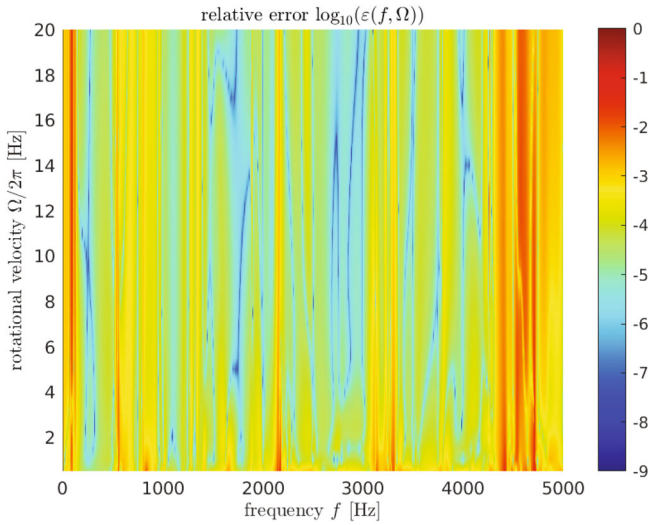

FIGURE 10 Relative error $\varepsilon(f, \Omega)$ of the transfer function of the parametrically reduced system.

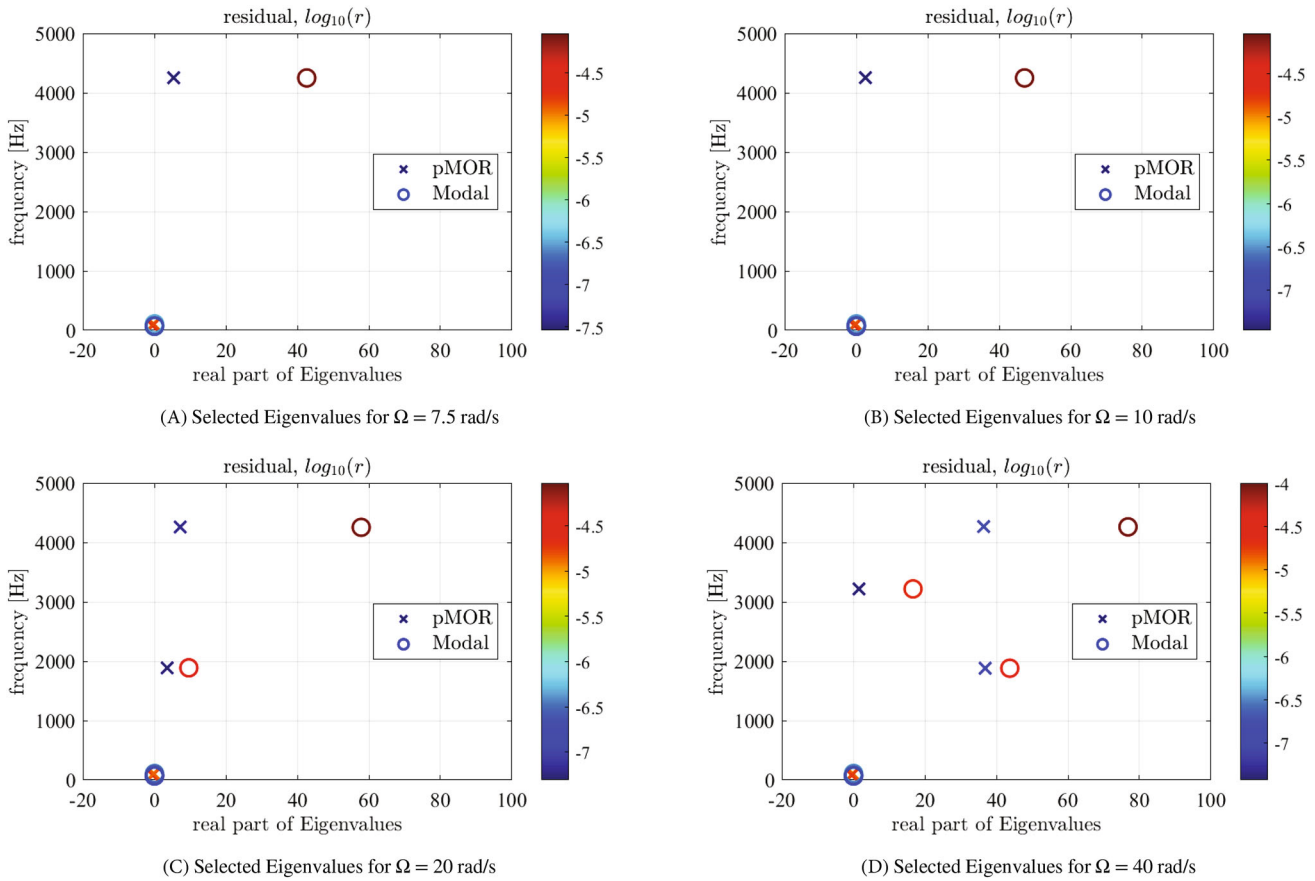

(A) Selected Eigenvalues for $\Omega = 7.5$ rad/s

(B) Selected Eigenvalues for $\Omega = 10$ rad/s

(C) Selected Eigenvalues for $\Omega = 20$ rad/s

(D) Selected Eigenvalues for $\Omega = 40$ rad/s

FIGURE 11 Selected eigenvalues for different speeds Ω_i and methods, color coded with the residual.

residual. At the rotational speed $\Omega = 7.5\,\text{rad/s}$ both methods find an eigenvalue with a positive real part at roughly $f = 4250\,\text{Hz}$, but the real parts are different. At this point it must be mentioned that the residual with the new method has a significantly smaller residual than the modal method. This can be identified by the color of the markers. The eigenvalues at roughly $f = 100\,\text{Hz}$ have a negative real part and are therefore assumed to be stable. When we compare these results with the transfer function in Figures 7 and 6, we notice that for the frequency $f = 4250\,\text{Hz}$ we can find a very strong peak. Below $f = 500\,\text{Hz}$ there is no high amplification in the transfer function recognizable. Thus, the stable behavior of the eigenvalues with negative real part at $f = 100\,\text{Hz}$ can also be confirmed. With increasing speed the eigenvalue shifts to a higher real parts, which means that it becomes more unstable, because the magnitude of the number is a measure of instability [15]. However, it remains the lower magnitude of the real part of the parametric reduced system. We can also find an increase of the peak at $f = 4250\,\text{Hz}$ in the transfer function in Figures 7 and 6 and can thereby assume that an increase of the peak in the transfer function correlates with a stronger unstable behavior.

At the speeds $\Omega = 20\,\text{rad/s}$ and $\Omega = 40\,\text{rad/s}$ respectively Figures 11C and 11D more eigenvalues with positive real part are detected from both methods. At $\Omega = 20\,\text{rad/s}$ in Figure 11C a new eigenvalue with $f = 1900\,\text{Hz}$ is detected and at $\Omega = 40\,\text{rad/s}$ even one more with $f = 3200\,\text{Hz}$ appears. In both cases the real part of the pMOR reduced system is smaller than from the modal system and the residual also behaves as at lower speed. Which means that the pMOR method assigns a lower tendency to unstable behavior to the eigenvalues than the modal method. Nevertheless, both methods predict instability. If we compare the Figures 11C and 11D with the transfer functions in Figures 7 and 6, we again recognize a corresponding peak in the transfer function at $f = 1900\,\text{Hz}$ and $f = 3200\,\text{Hz}$, which becomes more pronounced with increasing rotational speed. This confirms the observation that as the real part increases, an increasing gain can be seen in the transfer function. However, it is not possible to conclude from these investigations that a particular amplification belongs to an eigenvalue with a positive real part which yields unstable behavior.

By comparing the eigenvalues and the associated residuals, it was shown that the new method can be used to compute consistent results even for large models. Both methods deliver the same statement concerning stability in the considered range. However, the associated residual for the eigenvalues with positive real part is lower with the new method than with the modal reduction. For the eigenvalues around 100 Hz, the modal reduction delivers eigenvalues with smaller residual. Thus, it cannot be said across the board that the new method provides more accurate eigenvalues. One reason for the discrepancy of the real parts could be the consideration of damping when reducing the system with the pMOR method. It should be mentioned that the used reduction method is based on the approximation of the transmission behavior. In order to represent the eigenvalues with an even higher accuracy, it would be possible to reduce in two steps, in order to place the expansion points closer to the eigenfrequencies of the system and thus to represent the system in this area even better. Furthermore, it is very interesting that the eigenvalues which yield unstable behavior can be found in the transfer function and also the change of stability can be found in the transfer function.

5 | CONCLUSION

In this paper, an interpolation-based approach of model reduction based on moment matching methods for parametric systems has been successfully applied to an industrial brake system used for stability analysis. Instead of using eigenmodes of the undamped system for the reduction basis, in the workflow of complex eigenvalue analysis, the Krylov-subspace method is used to approximate the transfer behavior of the entire system. The computational effort required to generate the basis is higher as for the computation of eigenmodes, see Section 4. However, the new method also takes into account the damping effects or, more generally, parameter-dependent terms. The evaluation of the results has shown that the new method predicts the same stability behavior as the classical method. Thus, the method provides the same statement regarding the stability, but the damping rate tends to be lower. Furthermore, the residuals of the eigenvalues with positive real part are smaller than with the modal reduction. In addition to the eigenvalues, the transfer functions of the system were also considered. Here it became apparent that the new method is clearly superior to the modal reduction with a comparable reduced system size. Over the entire parameter space, a good approximation of the transfer function of the entire system is achieved, whereas with the modal reduction, an imprecise approximation of the transfer behavior is achieved. The comparison of both analyses also showed that the unstable eigenmodes can be found in the transfer function. The transfer behavior is highly amplified at these frequencies which leads to high peaks. It could also be shown that at certain unstable eigenfrequencies and increasing rotational speed and thus decreasing damping rate, the amplification in the transfer function also increases. This shows that in the analysis of oscillating systems not only the eigenvalues but also the transfer behavior is important. The computation time for creating the basis of the new method is longer than for

the modal reduction. However, compared to the total computing time for the calculation of the eigenvalues or transfer function this is negligible.

Furthermore, in this paper a lattice distribution of the expansion points s was chosen for the calculation of the basis with the Krylov method. In addition, only one input and one output of the system were used. In further investigations, the focus can be on an optimized choice of expansion points or an extended choice of inputs and outputs of the system in order to approximate the behavior of the system even better.

ACKNOWLEDGMENT

Open Access funding enabled and organized by Projekt DEAL.

REFERENCES

[1] A. Antoulas, *Approximation of large-scale dynamical systems*, SIAM, Philadelphia, PA, 2005.
[2] U. Baur, C. Beattie, P. Benner, and S. Gugercin, Interpolatory projection methods for parameterized model reduction, SIAM J Sci Comput **33** (2011), no. 5, 2489–2518.
[3] P. Benner, S. Gugercin, and K. Willcox, A survey of projection-based model reduction methods for parametric dynamical systems, SIAM Rev. **57** (2015), no. 4, 483–531.
[4] J. Fehr, "*Automated and error-controlled model reduction in elastic multibody systems*," *Dissertation, Schriften aus dem Institut für Technische und Numerische Mechanik der Universität Stuttgart*, Vol **21**, Shaker Verlag, Aachen, 2011.
[5] N. Gräbner, S. Quraishi, C. Schröder, V. Mehrmann, and U. von Wagner, "*New numerical methods for the complex eigenvalue analysis (CEA) of disk brake squeal*," *Proceedings of the Eurobrake conference*, Lille, France, 2014.
[6] N. Gräbner, V. Mehrmann, S. Quraishi, C. Schröder, and U. von Wagner, Numerical methods for parametric model reduction in the simulation of disk brake squeal, ZAMM: J Appl Math Mech **96** (2016), no. 12, 1388–1405.
[7] N. Gräbner, *Analyse und Verbesserung der Simulationsmethode des Bremsenquietschens*, Dissertation, Institut für Mechanik FG Mechatronische Maschinendynamik,Technische Universität Berlin, Berlin, Germany, 2016.
[8] W. Hahn, *Stability of motion*, Springer Verlag, Berlin, 1967.
[9] H. Hetzler, *Zur Stabilität von Systemen bewegter Kontinua mit Reibkontakten am Beispiel des Bremsenquietschens*, Dissertation, Karlsruhe Institute of Technology, Karlsruhe, Germany, 2008.
[10] INTES, *PERMAS product description version 18*, Intes GmbH, Stuttgart, 2020.
[11] I. Iroz, *Simulation of friction-induced vibrations in automotive brake systems*, Dissertation, Institute of Engineering and Computational Mechanics, University of Stuttgart, Stuttgart, Germany, 2017. Doctoral Dissertation. Schriften aus dem Institut für Technische und Numerische Mechanik der Universität Stuttgart, Vol **56**, Shaker Verlag, Aachen, 2017.
[12] H. Irretier, *Experimentelle Modalanalyse*, Institut für Mechanik, Universität Kassel, Kassel, 2004.
[13] N. Kinkaid, O. O'Reilly, and P. Papadopoulos, Automotive disc brake squeal, J. Sound Vib. **267** (2003), no. 1, 105–166.
[14] M. Lehner, *Modellreduktion in elastischen Mehrkörpersystemen (in German), Dissertation*, Vol **10**, Schriften aus dem Institut für Technische und Numerische Mechanik der Universität Stuttgart, Shaker Verlag, Aachen, 2007.
[15] G. Liles, Analysis of disc brake squeal using finite element methods, SAE Paper **98** (1989), no. 6, 1138–1146.
[16] F. Matter, B. Fröhlich, I. Iroz, and P. Eberhard, Investigations of disc brake squeal using model order reduction approaches for ther complex eigenvalue analysis. *Proceedings of the 27th international congress on sound and vibration (ICSV27)* 2021.
[17] H. Ouyang, W. Nack, Y. Yuan, and F. Chen, Numerical analysis of automotive disc brake squeal, Int. J. Veh. Noise Vib. **1** (2005), 207–231.
[18] E. Rabinowicz, *Friction and wear of materials*, John Wiley and Sons, New York, 1965.
[19] J. Rao, *Rotor dynamics*, New Age International, New Delhi, 1996.
[20] N. Walker, B. Fröhlich, and P. Eberhard, Model order reduction for parameter dependent substructured systems using Krylov subspaces, *IFAC-PapersOnLine, Special Issue on 9th Vienna International Conference on Mathematical Modelling*, vol. **51**, 553–558, https://doi.org/10.1016/j.ifacol.2018.03.093.
[21] K. Zhou, J. Doyle, and K. Glover, *Robust and optimal control*, Prentice Hall, Upper Saddle River, 1996.
[22] O. C. Zienkiewicz, R. L. Taylor, and J. Z. Zhu, *The finite element method: Its basis & fundamentals*, 7th ed., Butterworth-Heinemann, Oxford, 2013.

How to cite this article: F. Matter, I. Iroz, and P. Eberhard, *Interpolation-based parametric model order reduction of automotive brake systems for frequency-domain analyses*, GAMM-Mitteilungen. **46** (2023), e202300002. https://doi.org/10.1002/gamm.202300002